NOTICE

CERTAIN DATA CONTAINED IN THIS DOCUMENT MAY BE DIFFICULT TO READ IN MICROFICHE PRODUCTS.

UCRL-CR--103909

DE91 000946

THE PRESSURE RELAXATION OF LIQUID JETS AFTER ISOCHORIC HEATING

X.M. Chen and Virgil E. Schrock
Department of Nuclear Engineering
University of California at Berkeley
Berkeley, CA 94720
(415) 642-6431

Paper Proposed for
the Ninth Topical Meeting on Technology of
Fusion Energy

October 7-11, 1990, Oak Brook, IL

Work performed under the auspices of the U.S. Department of Energy by the Lawrence Livermore National Laboratory under contract W-7405-Eng-48

DISCLAIMER

Work performed under the auspices of the U.S. Department of Energy by Lawrence Livermore National Laboratory under contract number W-7405-ENG-48.

THE PRESSURE RELAXATION OF LIQUID JETS AFTER ISOCHORIC HEATING

X.M. Chen and V.E. Schrock
Department of Nuclear Engineering
University of California at Berkeley
Berkeley, CA 94720
(415) 642-6431

ABSTRACT

During isochoric heating by fast neutron irradiation, a high pressure is almost instantaneously built up inside the falling liquid jets in a HYLIFE (ICF) reactor. It has been suggested that the jets will breakup as a consequence of negative pressure occurring during the relaxation[1,2]. This is important to both the subsequent condensation process and the chamber wall design. In this paper the mechanism of the relaxation of liquid jets after isochoric heating has been studied with both incompressible and compressible models. The transient pressure field predicted is qualitatively similar for both models and reveals a strongly peaked tension in the wake of a rarefaction wave. The pressure then rises monotonically in radius to zero pressure on the boundary. The incompressible approximation greatly over predicts the peak tension, which increases with time as the rarefaction wave moves toward the center of the jet. Since the tension distribution is as a narrow spike rather than uniform, a cylindrical fracture is the most likely mode of failure. The paper also discusses the available methods for estimating liquid tensile strength.

INTRODUCTION

The HYLIFE design study[3] considered the possibility that isochoric heating of neutron absorbing liquid jets would cause fragmentation of the liquid. It was recognized that the relaxation of the initial high liquid pressure would produce tension within an outward radial flow. However, the flow field during relaxation was not analyzed but rather an implicit assumption was that tension occurs uniformly throughout the liquid. As a part of the current HYLIFE-II study (molten salt Flibe replacing lithium) we have analyzed the velocity and pressure fields using incompressible and compressible fluid models in order to gain greater insight into the fragmentation problem. Results of the incompressible model, which assumes the liquid is incompressible everywhere except at a thin wave front, were presented previously[4]. It was found that a sharp peak tension occurs immediately behind the advancing rarefaction wave and the pressure then rises monotonically in radius to zero on the boundary. The magnitude of the instantaneous peak tension increases very rapidly as the wave approaches the center of the cylindrical jet and depending on the initial pressure, the liquid may fracture.

Because there is a sharp peak in the tension, it appears that fracture will most likely occur in a cylindrical surface. Such a fracture would set free an annulus of liquid which is in outward radial motion with zero pressure on both boundaries. As the rarefaction wave continues into the undisturbed core of the fluid the process is repeated so that the cylinder may break into a series of liquid annuli (similar to sections of an onion).

The incompressible model is not exact. We know that rarefaction waves tend to broaden as the move and the wave does not appear as a discontinuity. Also the range of pressures predicted suggest that the motion is affected by compressibility. For this reason we have developed a compressible model for the problem.

COMPRESSIBLE FLUID MODEL

Work performed under the auspices of the US Department of Energy by the Lawrence Livermore National Laboratory under Contract W-7405-Eng-48

Figure 1. The Description of the Relaxation Jet

The relaxation process begins with the liquid cylindrical region at a uniform high pressure induced by uniform (assumed) neutron pulsed heating (see Figure 1). The leading edge of a rarefaction wave moves at the sound speed C toward the center of the cylinder. Thus, at any instant, we have an undisturbed cylindrical core (region I) and an annular zone (region II) that has experienced expansion and is moving radially outward. The motion is region II is one dimensional and the governing conservation equations are therefore the following[5]

Mass

$$\frac{\partial \rho}{\partial t}+\frac{1}{r}(\rho r V_r)=0 \qquad (1)$$

Radial Momentum

$$\rho\left(\frac{\partial V_r}{\partial t}+V_r\frac{\partial V_r}{\partial r}\right)=-\frac{\partial P}{\partial r} \qquad (2)$$

where viscosity is neglected.

The relationship between density and pressure during an isentropic process may be expressed as

$$\rho=\rho(P,S_0) \quad . \qquad (3)$$

Initial and boundary conditions are:

I.C.

$$P(r)=P_\infty \qquad r \le R_0 \qquad (4a)$$

$$\rho(r)=\rho_\infty \qquad r \le R_0 \qquad (4b)$$

$$V_r(r)=0, \qquad r < R_0 \qquad (4c)$$

B.C.

$$P(R,t)=0 \qquad (5a)$$

$$\frac{\partial P(0,t)}{\partial r}=0 \qquad (5b)$$

Following Chaudhry[6] we introduce the sound speed

$$C=\sqrt{\frac{K}{\rho}}=\sqrt{\frac{dP}{d\rho}} \qquad (6)$$

where K is the bulk modules of elasticity of the liquid. The continuity Equation 1 becomes, since we have $V/C \ll 1$,

$$\frac{\partial P}{\partial t}+\rho C^2\frac{\partial V_r}{\partial r}+\rho C^2\frac{V_r}{r}=0 \quad . \qquad (7)$$

Similarly the momentum equation reduces to

$$\rho\frac{\partial V_r}{\partial t}=-\frac{\partial P}{\partial r} \qquad (8)$$

The equations are then solved numerically.

NUMERICAL SOLUTION METHOD

The Gabutti scheme[7] is a suitable method for the numerical solution of compressible relaxation. In this scheme, the governing equations are first transformed into the characteristics form and the partial derivatives are replaced by the finite difference approximations. The scheme is comprised of two steps: predictor and corrector. The predictor part is further subdivided into two parts.

By adding Equation 8 to the product of Equation 7 and η, we have

$$\left(\frac{\partial P}{\partial t}+\frac{\eta}{\rho}\frac{\partial P}{\partial r}\right)+\eta\left(\frac{\partial V_r}{\partial t}+\frac{\rho C^2}{\eta}\frac{\partial V_r}{\partial r}\right)+\rho C^2\frac{V_r}{r}=0 \quad . (9)$$

Let $$\eta/\rho = dr/dt = \rho C^2/\eta \quad . \qquad (10)$$

It follows from this equation that the characteristic directions are:

$$\lambda^+ = dr/dt = +C \qquad (11)$$

$$\lambda^- = dr/dt = -C \quad . \qquad (12)$$

After further combination and simplification we obtain the characteristic equations

$$\frac{\partial P}{\partial t}+0.5\left(\lambda^+\frac{\partial P^+}{\partial r}+\lambda^-\frac{\partial P^-}{\partial r}\right)$$

$$+0.5\rho C\left(\lambda^+\frac{\partial V_r^+}{\partial r}-\lambda^-\frac{\partial V_r^-}{\partial r}\right)+\rho C^2\frac{V_r}{r}=0 \quad . \qquad (13)$$

and

$$\frac{\partial V_r}{\partial t}+0.5\left(\lambda^+\frac{\partial V_r^+}{\partial r}+\lambda^-\frac{\partial V_r^-}{\partial r}\right)$$

$$+\frac{0.5}{\rho C}\left(\lambda^+\frac{\partial P^+}{\partial r}-\lambda^-\frac{\partial P^-}{\partial r}\right)=0 \quad . \qquad (14)$$

in which the superscripts indicate the characteristic directions along which the derivative are to be approximated.

Substitution of finite difference approximations for the time derivatives into equations (13) and (14) yields the predicted values of V_i^* and P_i^*:

$$P_i^* = P_i^l - 0.5\Delta t\left(\lambda^+\frac{\partial P^+}{\partial r}+\lambda^-\frac{\partial P^-}{\partial r}\right)$$

$$-0.5\rho C\,\Delta t\left(\lambda^+\frac{\partial V_r^+}{\partial r}-\lambda^-\frac{\partial V_r^-}{\partial r}\right)-\rho C^2\frac{V_r}{r}\Delta t \qquad (15)$$

$$V_i^* = V_i^l - 0.5\Delta t\left(\lambda^+\frac{\partial V_r^+}{\partial r} + \lambda^-\frac{\partial V_r^-}{\partial r}\right)$$

$$-\frac{0.5}{\rho C}\Delta t\left(\lambda^+\frac{\partial P^+}{\partial r} - \lambda^-\frac{\partial P^-}{\partial r}\right) \qquad (16)$$

The spatial derivatives in Equation (15) and (16) are approximated as follows.

Predictor Part

Part 1: Calculating the predicted values of P_i^* and V_i^* which are going to be used in the corrector part. In this part, the following finite-difference approximations are used to determine the values of P_i^* and V_i^* from equation (15) and (16):

$$\frac{\partial F^+}{\partial r} = \frac{F_i^l - F_{i-1}^l}{\Delta r} \qquad (17)$$

$$\frac{\partial F^-}{\partial r} = \frac{F_{i+1}^l - F_i^l}{\Delta r} \qquad (18)$$

Part 2: To determine the predicted values of time derivatives $\partial P^*/\partial t$ and $\partial V^*/\partial t$ in equation (13) and (14) the following finite-difference approximations are used:

$$\frac{\partial F^+}{\partial r} = \frac{2F_i^l - 3F_{i-1}^l + F_{i-2}^l}{\Delta r} \qquad (19)$$

$$\frac{\partial F^-}{\partial r} = \frac{-2F_i^l + 3F_{i+1}^l - F_{i+2}^l}{\Delta r} \qquad (20)$$

Correct Part

In this part, we want to find the other set of $\partial P/\partial t$ and $\partial V/\partial r$. This time the derivatives $\partial V/\partial r$ and $\partial P/\partial r$, take the finite-difference approximations shown below and P^* and V^* are from (15) and (16).

$$\frac{\partial F^+}{\partial r} = \frac{F_i^* - F_{i-1}^*}{\Delta r} \qquad (21)$$

$$\frac{\partial F^-}{\partial r} = \frac{F_{i+1}^* - F_i^*}{\Delta r} \qquad (22)$$

Then the values of V and P at the new time are determined from the following equations:

$$P_i^{l+1} = P_i^l + 0.5\Delta t\left(\frac{\partial P^*}{\partial t} + \frac{\partial P}{\partial t}\right) \qquad (23)$$

$$V_i^{l+1} = V_i^l + 0.5\Delta t\left(\frac{\partial V^*}{\partial t} + \frac{\partial V}{\partial t}\right). \qquad (24)$$

Note that the above discretization is possible only at nodes 3,4,...., n-2 during part 2 of the predictor step. One sided differences are used at nodes 2 and n-1.

Boundary conditions

In our problem, the border is changing with time. When the surface velocity is positive the size R is increasing; otherwise it is decreasing. It can be determined by

$$R(t+\Delta t) = R(t) + V(R,t)\Delta t \quad . \qquad (25)$$

From Equation 17, we have two one-sided finite-difference equations at $\lambda = \pm\rho C$ Equations 21 and 22. At the downstream end we can make use of Equation 21, while at the upstream end Equation 22 can be used. In our problem, the surface is the only interface with surrounding. It is "downstream" in terms of the fluid velocity direction. So, Equation 21 is used for surface nodes with the knowledge that $\partial P/\partial t = 0$. Thus we have

$$\partial V/\partial t = -\frac{1}{\rho}\frac{\partial P^*}{\partial r} - \lambda^+\frac{\partial V_r^+}{\partial r} - C\frac{V_r}{r}. \qquad (26)$$

At the center of the jet the pressure profile must be symmetrical. And the fluid velocity must be zero. That is to say

$$P(\Delta r) = P(-\Delta r) \qquad (27)$$

$$V(r=0) = 0$$

We must also notice that during the predictor part we can not write out the forward finite-difference at the downstream boundary (nor the backward finite-difference at the upstream), i.e., in order to solve a boundary node n we must have the values at the node $n+1$. To solve this problem, we need to extrapolate the boundaries by assuming fictitious nodes beyond the boundaries. The fictitious values of pressure and velocity can be extrapolated using the following equations[4]:

$$f_{n+1}^l = 2f_n^l - f_{n-1}^l \qquad (28a)$$

$$f_0^l = 2f_1^l - f_2^l \quad . \qquad (28b)$$

Now we can use the finite-difference equations at the boundary nodes 1 and n.

RESULTS OF COMPRESSIBLE ANALYSIS AND COMPARISON WITH INCOMPRESSIBLE ANALYSIS

From Figure 2, we can see that the pressure history within the relaxing jet is similar to the incompressible analysis result shown in Figure 3. The liquid behind the rarefaction wave front is in negative pressure (tension) domain. As the process proceeds, the tension at a local position does not change much. But the tension right behind the wave front is increasing steadily as the wave front proceeds. As a characteristic of rarefaction wave propagation we can also see that the wave front is broadening in Figure 2. The incompressible analysis obviously can not show this feature.

Although both compressible and incompressible analysis have the similar shapes of pressure profile, the magnitude of the tension in liquid is different. The incompressible model over predicts the magnitude of the tension. The predicted peak tensions are compared in Figure 4 where peak tension is plotted as a function of the position of the peak. It is seen that error in the

Figure 2. The Pressure History of Compressible Analysis

Figure 3. The Pressure History of Incompressible Model

Figure 4. The Comparison of Local Peak Tension

incompressible result increases at an ever increasing rate. The incompressible theory predicts infinite tension when the wave reaches the center of the cylinder while a finite maximum value is predicted by the compressible theory at a time shortly after the wave reflects as an outward moving shock. The transient fluid velocity predicted by the compressible model is

Figure 5. The Transient Velocity from Compressible Model

shown in Figure 5 and the surface acceleration rates by the two models are compared in Figure 6. More comparisons may be found in reference [9].

Figure 6. The Comparison of the Surface Accelerations

LIQUID FRAGMENTATION CONSIDERATIONS

Both incompressible and compressible models gives pressure profiles which suggest that the liquid will fail in a cylindrical fracture mode. The compressible theory is considered to give accurate quantitative results for transient pressure field. The tension limit is bounded by the thermodynamic limit of metastability (spinodal)[10]. We have shown that for a pure liquid the spinodal is equivalent to homogeneous nucleation. This may be useful in the case of a complex liquid such as Flibe for which the equation of state is not known. In any case, experiment have shown that most liquids fracture at tensions considerably lower than that at the spinodal[10]. Consequently experiments on Flibe are need to establish its tensile strength.

Another possible mechanism of liquid fragmentations Taylor like surface instabilities. Plesset[11] derived the conditions of stability for an accelerating spherical surface. Chen and Schrock recently applied the same method to obtain the conditions for a cylindrical surface[12]. These conditions indicate that there will not be fragmentation due to surface instability. In a companion paper on motion of a free annulus[13] we discuss this further.

CONCLUSIONS

The relaxation of an isochorically heated cylindrical column of liquid has been analyzed. The predicted transient pressure profiles show that the liquid is likely to fracture in a cylindrical surface rather than fragment homogeneously as previously thought. Experiments are needed to establish the tensile strength of candidate liquids.

REFERENCES

1. J.A. Blink, "Fragmentation of Suddenly Heated Liquids," Doctoral Thesis, University of California, Davis (1985).

2. L.A. Glenn, "On the Motion Following Isochoric Heating of Concentric Liquid Annuli," Nuclear Engineering and Design 60 pp 327-337 (1980).

3. J.A. Blink, et. al., "The High-Yield Lithium-Injection Fusion-Energy (HYLIFE) Reactor," Lawrence Livermore National Laboratory, UCRL-53559 (1985).

4. X.M. Chen and V.E. Schrock, "On the Relaxation of a Liquid Jet after Isochoric Heating," Trans. ANS, 60, pp174-175 (1989).

5. R.B. Bird, W.E. Stewart and E.N. Lightfoot, "Transport Phenomena," John Wiley and Sons, Inc. (1960).

6. M.H. Chaudhry and V. Yuvjevich, "Closed-Conduct Flow," Water Resource Publications by BookCrafters, Inc., USA (1981).

7. B. Gabutti, "On Two Upwind Finite-Difference Schemes for Hyperbolic Equations in Non-Conservation Form," Computers and Fluids 11 pp207-230 (1983).

8. M.H. Chaudhry and M.Y. Hussaini, "Second-Order Accurate Explicit finite-Difference Schemes for Waterhammer Analysis," Journal of Fluids Engineering 107 pp523-529 (1985).

9. X.M. Chen and V.E. Schrock, "The Pressure Relaxation of Liquid Jets After Isochoric Heating," University of California at Berkeley Report, UCB-NE-4155 (1989).

10. V.P. Skripov, "Metastable Liquids," Translation edited by D Slutzkin, John Wiley and Sons, Inc. (1972).

11. M.S. Plesset, "On the Stability of Fluid Flows with Spherical Symmetry," Journal of Applied Physics, 25 pp193-196, (1950).

12. X.M. Chen and V.E. Schrock, "On the Stability of a Cylindrical Interface of a Symmetric Flow," University of California at Berkeley Report, UCB-NE-4174, (1990).

13. X.M. Chen and V.E. Schrock, "A Note on the Pressure Field within an outward Moving Free Annulus," Nineth Fusion Topic Meeting at Chicago, (1990).

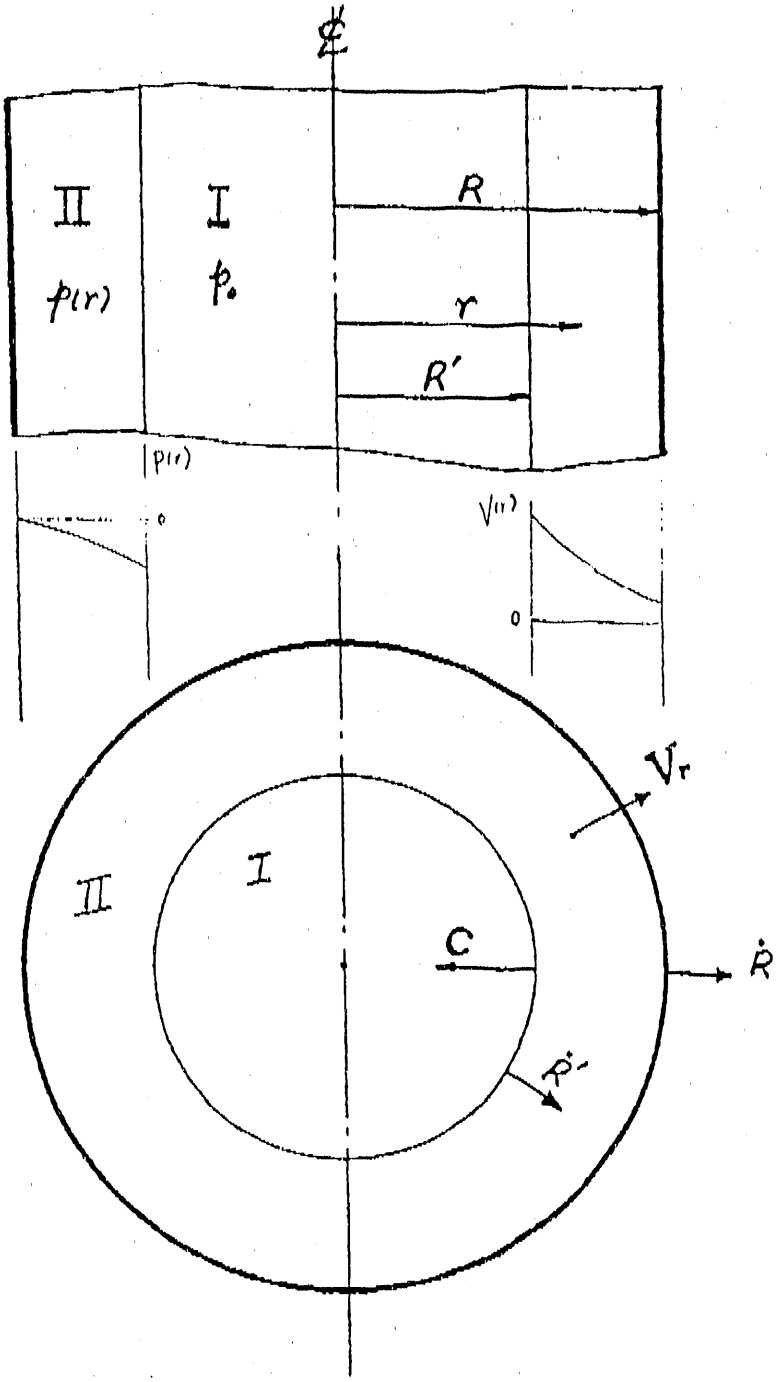

Fig. 1 Discription of Relaxation Model

Pressure Distribution (compressible)

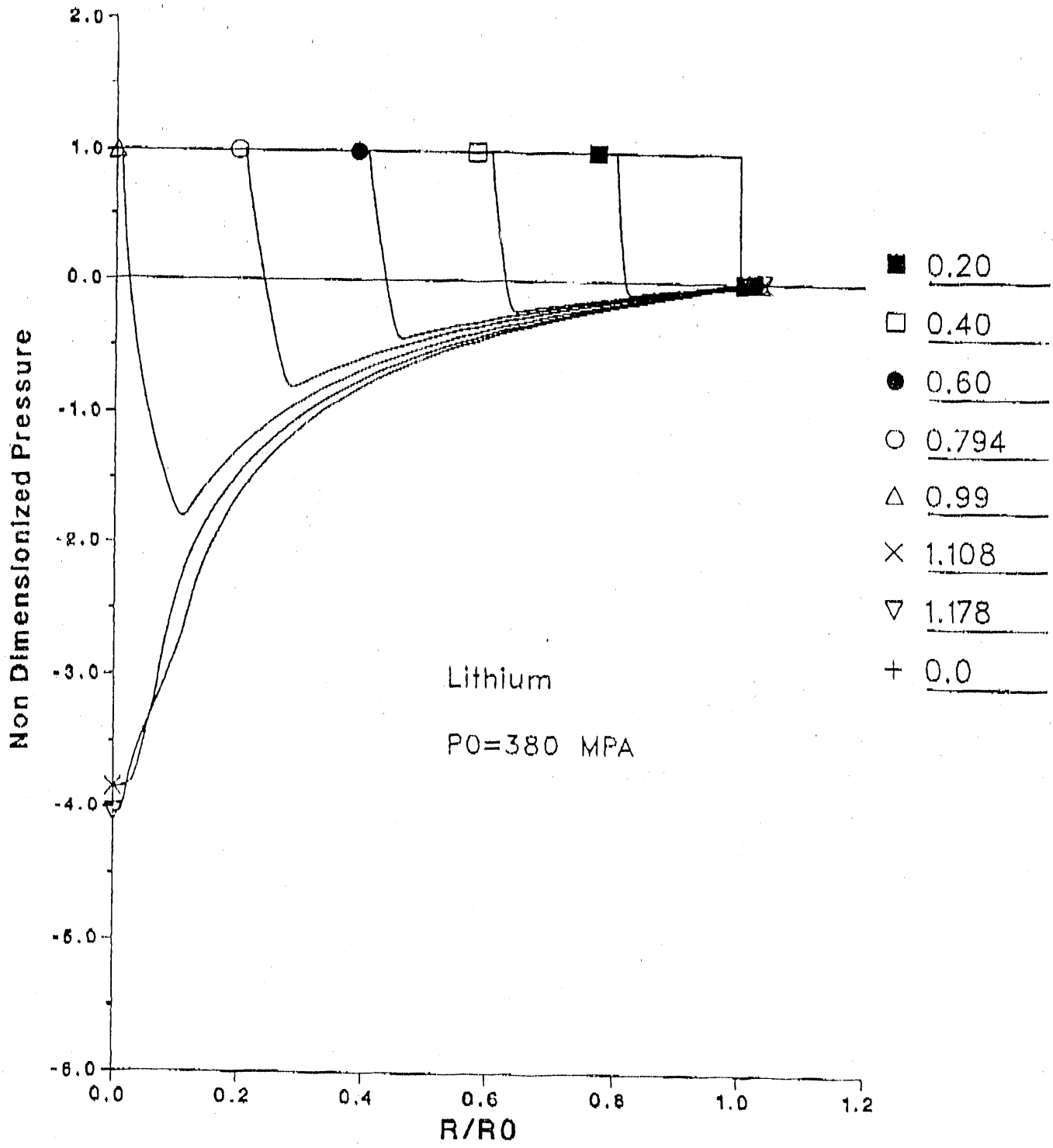

Fig. 2

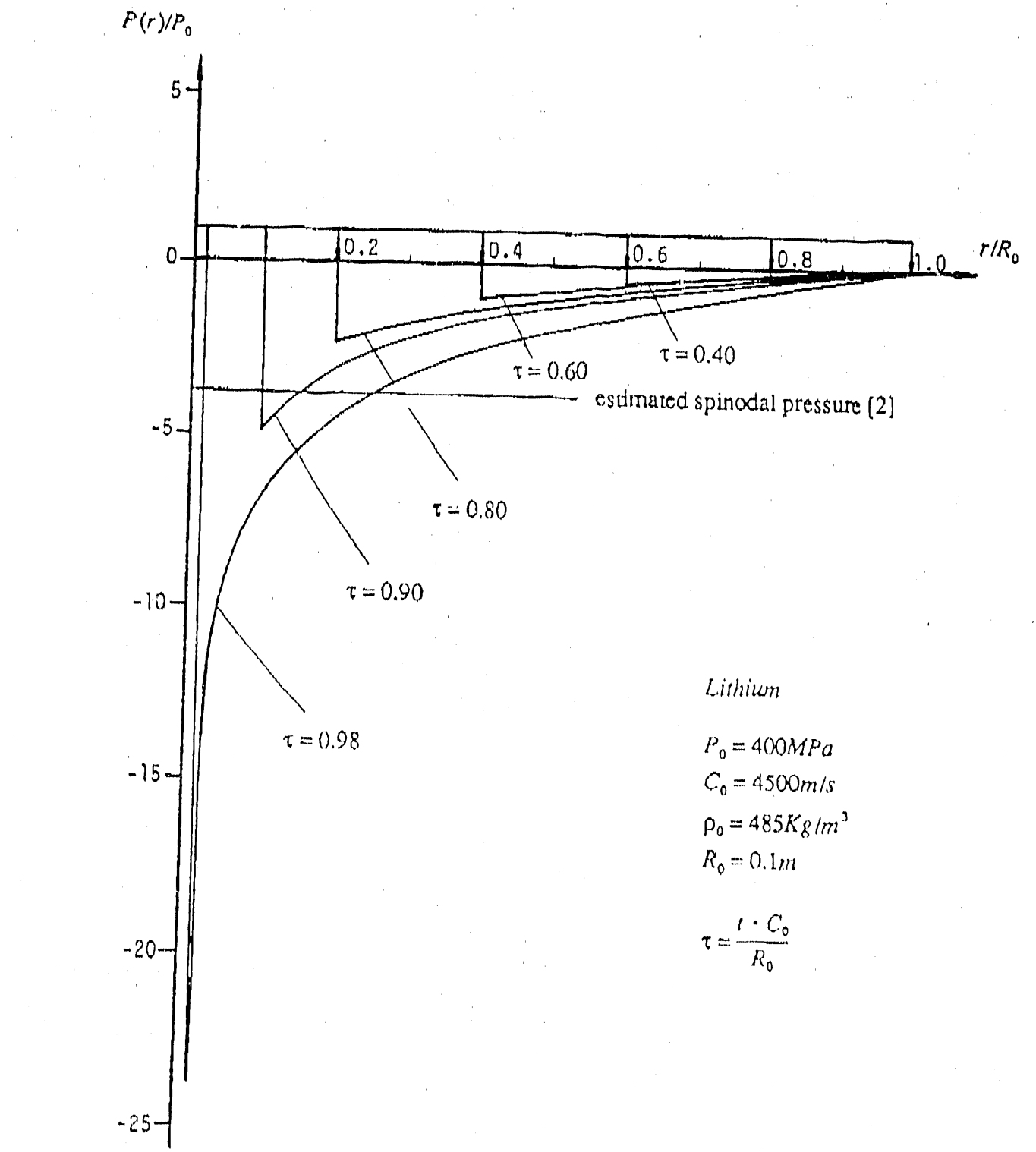
P(r)/P0
5
0
-5
-10
-15
-20
-25
0.2
0.4
0.6
0.8
1.0
r/R0
τ = 0.40
τ = 0.60
estimated spinodal pressure [2]
τ = 0.80
τ = 0.90
τ = 0.98
Lithium
P0 = 400MPa
C0 = 4500m/s
ρ0 = 485Kg/m3
R0 = 0.1m
τ = t · C0 / R0

Fig. 3

Peak Tension Comparison

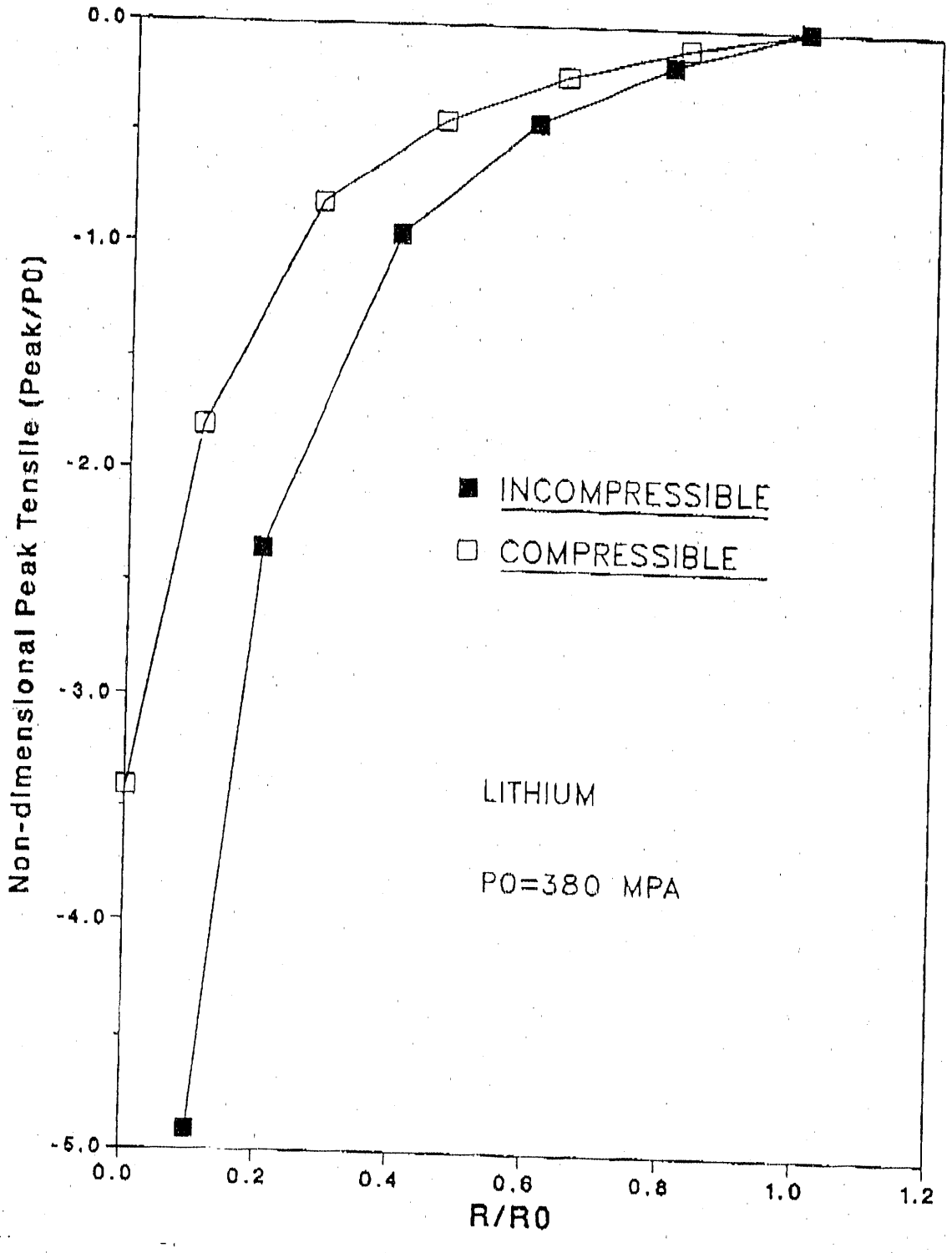

Fig. 4

Velocity Distribution (compressible)

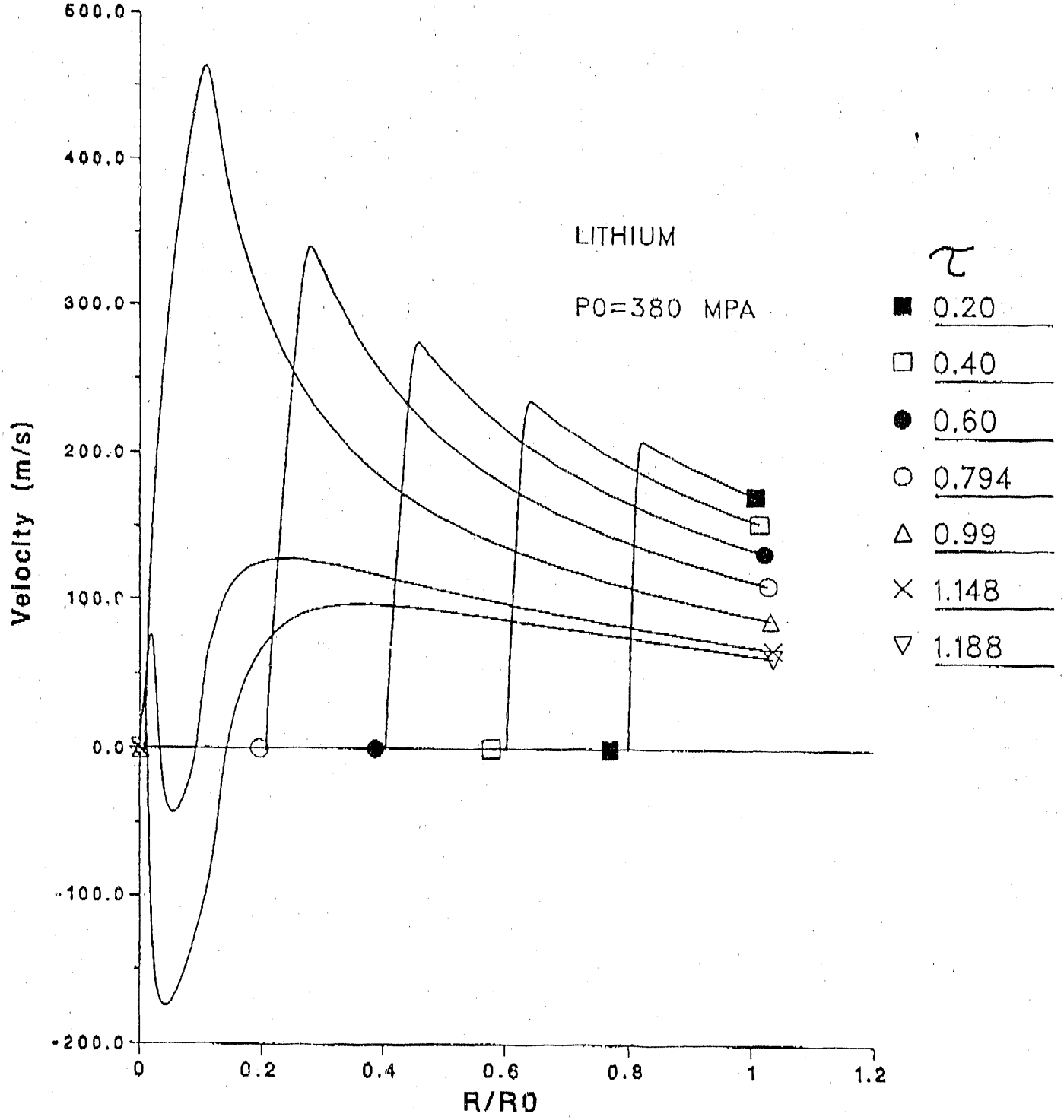

Fig. 5

SURFACE ACCELERATION HISTORY

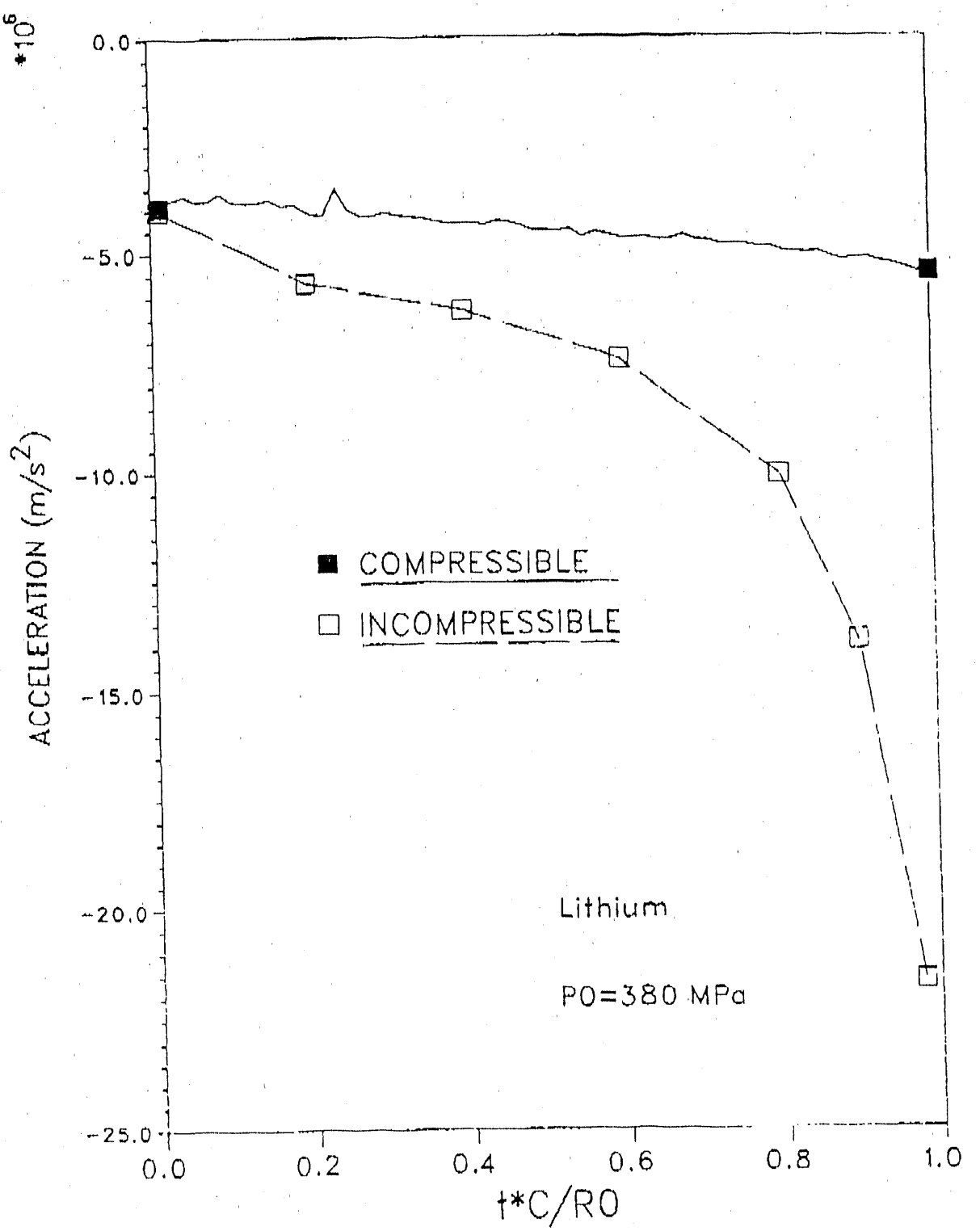

Fig. 6

- END -

DATE FILMED

11 / 05 / 90